

SERS activity of carbon nanotubes modified by silver nanoparticles with different particle sizes

Xiao-Lei Zhang(张晓蕾)[1,2,†], Jie Zhang(张洁)[3], Yuan Luo(罗元)[1], and Jia Ran(冉佳)[1,2]

Citation: Chin. Phys. B, 2022, 31 (**7**): 077401. DOI: 10.1088/1674-1056/ /ac4f51
Journal homepage: http://cpb.iphy.ac.cn; http://iopscience.iop.org/cpb

What follows is a list of articles you may be interested in

Photothermal-chemical synthesis of P-S-H ternary hydride at high pressures

Tingting Ye(叶婷婷), Hong Zeng(曾鸿), Peng Cheng(程鹏), Deyuan Yao(姚德元), Xiaomei Pan(潘孝美), Xiao Zhang(张晓), and Junfeng Ding(丁俊峰)

Chin. Phys. B, 2022, 31 (**6**): 067402. DOI: 10.1088/1674-1056/ac5604

Low-energy (40 keV) proton irradiation of $YBa_2Cu_3O_{7-x}$ thin films:Micro-Raman characterization and electrical transport properties

San-Sheng Wang(王三胜), Fang Li(李方), Han Wu(吴晗), Yu Zhang(张玉), Suleman Mu?ammad(穆罕默德苏尔曼), Peng Zhao(赵鹏), Xiao-Yun Le(乐小云), Zhi-Song Xiao(肖志松), Li-Xiang Jiang(姜利祥), Xue-Dong Ou(欧学东), Xiao-Ping Ouyang(欧阳晓平)

Chin. Phys. B, 2019, 28 (**2**): 027401. DOI: 10.1088/1674-1056/28/2/027401

Quantitative analysis of ammonium salts in coking industrial liquid waste treatment process based on Raman spectroscopy

Ya-Nan Cao(曹亚南), Gui-Shi Wang(王贵师), Tu Tan(谈图), Ting-Dong Cai(蔡廷栋), Kun Liu(刘锟), Lei Wang(汪磊), Gong-Dong Zhu(朱公栋), Jiao-Xu Mei(梅教旭)

Chin. Phys. B, 2016, 25 (**10**): 107403. DOI: 10.1088/1674-1056/25/10/107403

High-pressure Raman study of solid hydrogen up to 300 GPa

Xiaoli Huang(黄晓丽), Fangfei Li(李芳菲), Yanping Huang(黄艳萍), Gang Wu(吴刚), Xin Li(李鑫), Qiang Zhou(周强), Bingbing Liu(刘冰冰), Tian Cui(崔田)

Chin. Phys. B, 2016, 25 (**3**): 037401. DOI: 10.1088/1674-1056/25/3/037401

First-principles simulation of Raman spectra and structural properties of quartz up to 5 GPa

Liu Lei, Lv Chao-Jia, Zhuang Chun-Qiang, Yi Li, Liu Hong, Du Jian-Guo

Chin. Phys. B, 2015, 24 (**12**): 127401. DOI: 10.1088/1674-1056/24/12/127401

SERS activity of carbon nanotubes modified by silver nanoparticles with different particle sizes

Xiao-Lei Zhang(张晓蕾)[1,2,†], Jie Zhang(张洁)[3], Yuan Luo(罗元)[1], and Jia Ran(冉佳)[1,2]

[1] *Chongqing Municipal Level Key Laboratory of Photoelectronic Information Sensing and Transmitting Technology, College of Optoelectronic Engineering, Chongqing University of Posts and Telecommunications, Chongqing* 400065, *China*

[2] *Postdoctoral Research Center of Chongqing Key Laboratory of Optoelectronic Information Sensing and Transmission Technology, Chongqing University of Posts and Telecommunications, Chongqing* 400065, *China*

[3] *Key Laboratory of Optoelectronic Technology & System, Ministry of Education, College of Optoelectronic Engineering, Chongqing University, Chongqing* 400044, *China*

(Received 15 December 2021; revised manuscript received 19 January 2022; accepted manuscript online 27 January 2022)

A two-dimensional (2D) surface-enhanced Raman scattering (SERS) substrate is fabricated by decorating carbon nanotube (CNT) films with Ag nanoparticles (AgNPs) in different sizes, via simple and low-cost chemical reduction method and self-assembling method. The change of Raman and SERS activity of carbon nanotubes/Ag nanoparticles (CNTs/AgNPs) composites with varying size of AgNPs are investigated by using rhodamine 6G (R6G) as a probe molecule. Meanwhile, the scattering cross section of AgNPs and the distribution of electric field of CNTs/AgNPs composite are simulated through finite difference time domain (FDTD) method. Surface plasmon resonance (SPR) wavelength is redshifted as the size of AgNPs increases, and the intensity of SERS and electric field increase with AgNPs size increasing. The experiment and simulation results show a Raman scattering enhancement factor (EF) of 10^8 for the hybrid substrate.

Keywords: Raman spectroscopy, surface-enhanced Raman scattering (SERS), carbon nanotubes, silver nanoparticles

PACS: 74.25.nd, 78.30.–j, 36.20.Ng **DOI:** 10.1088/1674-1056/ac4f51

1. Introduction

The Raman scattering effect can reveal the internal structure information of substances through utilizing spectroscopy and provide a new and effective method to investigate the crystals and other substances.[1] Nevertheless, the difficulty in detecting the Raman spectrum is that the cross-sectional area of ordinary molecules is so small that the Raman signal is hard to be detected. Until 1974, the phenomenon of surface-enhanced Raman scattering (SERS) on the rough silver electrode surface was discovered by Fleischmann *et al.*,[2] and it has been found to possess important applications in environmental monitoring,[3,4] food safety,[5–7] chemical and biological sensing.[8,9] The SERS provides rich molecule fingerprint information through vibrational spectra, and exhibits high sensitivity, arriving at a single-molecule detection level. Additionally, it also overcomes the shortcomings of the traditional Raman spectroscopy, such as weak signal intensity and easy to interfer by fluorescence.[2,10,11] Meanwhile, it has the advantages, pretreatment-free, non-invasive, and non-destructive. It is generally accepted that there are two enhancement mechanisms: electromagnetic enhancement (10^6–10^8) and chemical enhancement (10^1–10^2).[12,13] The electromagnetic enhancement effect amplifies the Raman signal of molecules nearby target by enhancing the electric fields, which is caused by exciting the localized surface plasmon resonance (LSPR) of rough metal nanostructures. Metallic nanosystems possess collective excitations of their free electrons that are known as localized surface plasmons. They give rise to tightly focused and very intense near-fields that enhance optical processes.[14] The chemical enhancement effect is based on the interaction between the organic molecules and the nano-metallic structures, offering a weak enhancement. In general, the SERS enhancement is dominated by plasmonic properties of the metal nanostructures, which involves not only the metal material, but also the size, shape, and inter-particle coupling of the nanoparticles.

Various types of SERS substrates consisting of bare metal nanostructures are fabricated and discussed. It is known that nanospheres with different sizes may present different LSPR wavelengths, and SERS activity increases as the excitation wavelength approaches to the LSPR wavelength. Hence, it is significant to study the effect of metal nanoparticle sizes on SERS properties. In 2016, Lin *et al.*[15] systematically investigated the effect of structural parameters on SERS of individual gold nanorods. Benz *et al.*[16] analyzed the SERS property of individual nanoparticles on a mirror, and found that the total SERS intensity from a few hundred molecules under each nanoparticle dramatically increases with particle size increasing. In 2014, Cassar *et al.*[17] synthesized the monodispersed silver nanoparticles (AgNPs) with various sizes, used rhodamine 6G (R6G), malachite green and thiophenol as three analytes, and analyzed the SERS activity.

[†]Corresponding author. E-mail: zhangxiaolei@cqupt.edu.cn

© 2022 Chinese Physical Society and IOP Publishing Ltd

These studies analyzed the effect of metal nanoparticle size on SERS intensity of bare metal nanostructure. However, there are some disadvantages associated with a metallic substrate, such as major flaws in stability and reproducibility induced by oxidation. Moreover, the mere metal SERS substrates are hardly reusable as most of the metal-based SERS substrates are disposable. Recently, two-dimensional (2D) nanomaterials have attracted wide interest for their ability to resolve the problems of metallic NPs due to their excellent physical and chemical properties, and some SERS substrates where nanomaterials are decorated by metal nanoparticles have been investigated, such as graphene/AgNPs,[18–21] GO/AgNPs,[22] rGO/TiO_2/AgNPs,[23] ZnO/graphene/AgNPs,[24] Au/MoS_2 nano-array,[25] black phosphorus/Au NPs,[26] and CFC/AgNPs.[27] Compared with other 2D SERS materials, carbon nanotube (CNT) has a huge specific surface area, which can adsorb more nanoparticles and probe molecules; meanwhile, it has excellent molecular adsorption capacity, which can greatly reduce the effects of fluorescent background of the SERS signal and quench the photoluminescence of fluorescent dyes.[28] More importantly, the CNT structure is a good choice as plasmonic component to meet the requirements for intensive light scattering properties.[29] The plasmonic properties of CNTs have been studied on individual tubes coated by silver nanoparticles (AgNPs),[30] AgNPs/CNT nanohybrids,[31] AuNPs/MWCNTs,[32] and Au/Ag nanoparticle/carbon nanotube.[33] However, few researches of the influence of the metal nanoparticles' sizes on SERS activity of composite structures have been conducted.

In this paper, we synthesize sliver nanoparticles with different sizes by a simple and low-cost chemical reduction method. The sliver nanoparticles are self-assembled with carbon nanotubes to form the carbon nanotubes/Ag nanoparticles (CNTs/AgNPs) SERS substrate. The R6G molecule acts as an analyst probe to analyze the SERS activity of the substrate. Additionally, combining the characterization results from the scanning electron microscopy (SEM), the theoretical simulations are further performed.

2. Experimental preparation and characterization

2.1. Experimental preparation

Figure 1 shows schematically the preparation process of CNTs/AgNPs composite samples, including the preparation of CNTs suspension, Ag sol and CNTs/AgNPs.

2.1.1. Preparation of carbon nanotube suspension

The CNT powder (the main range of the diameter: 40 nm∼60 nm; length: < 2 μm; purity: $> 97\%$, commercial product from Shenzhen Nanotech Port Co., Ltd.) and triton X-100 were dispersed into deionized water. The resulting solution was stirred with a glass rod for 5 min then ultrasonically oscillated for 4 h to obtain CNT suspension with a concentration of 0.5 mg/mL.

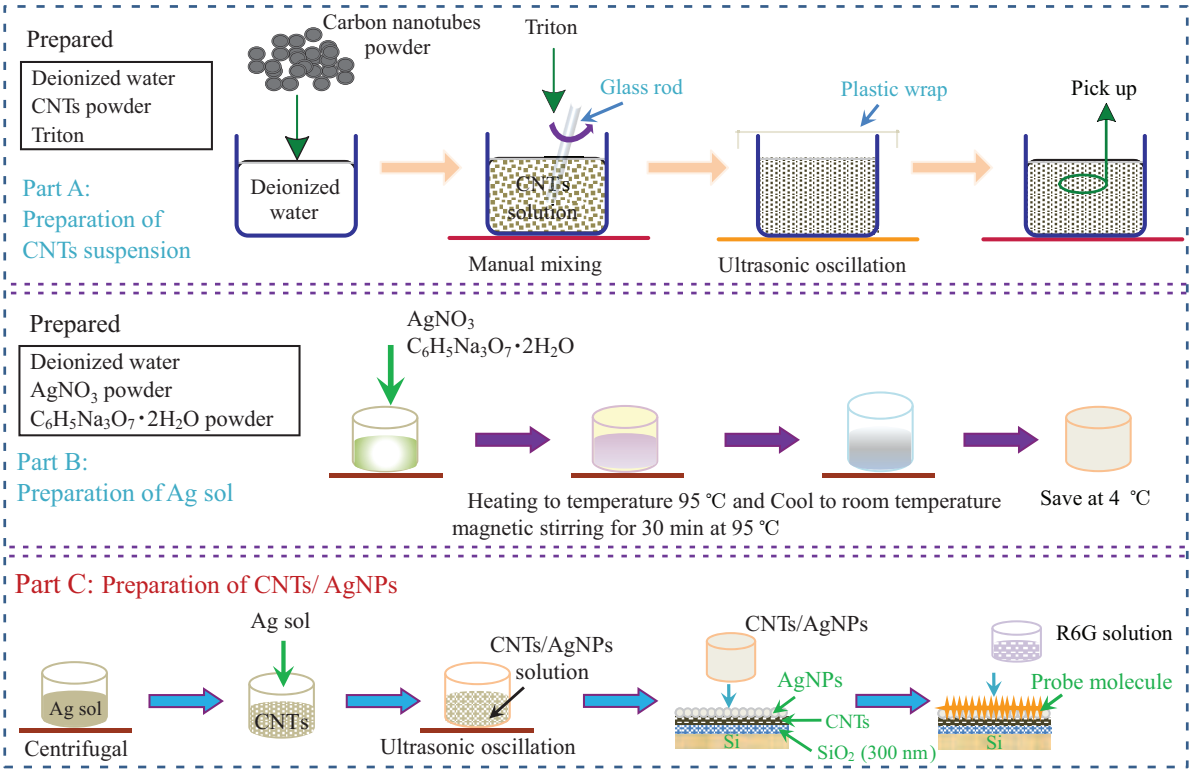


Fig. 1. Scheme of fabrication process of CNTs/AgNPs SERS substrate.

2.1.2. Preparation of Ag sol solution

The chemical reduction method of Ag sol solution was used.[34] Firstly, 17-mg silver nitrate ($AgNO_3$) was added into 100-mL deionized water. Secondly, the above mentioned solution was placed on a magnetic stirrer and heated to boiling temperature (about 95 °C). Thirdly, different amounts of sodium citrate ($C_6H_5Na_3O_7{\cdot}2H_2O$) were rapidly added into the above solution, the mixture solution was kept at boiling temperature for 30 min with vigorous stirring. Finally, the reacted solution (Ag sol) was naturally cooled to room temperature, then sealed and stored in a refrigerator at 4 °C. In our experiments, the amounts of sodium citrate used ranged from 25 mg to 5 mg, which resulted in AgNPs with diameters from 44 nm to 59 nm.

2.1.3. CNTs/AgNPs synthesis

Firstly, the prepared Ag sol solution was centrifuged at a speed of 4000 r/min for 60 min in order to separate from the impurities. Then, the separated AgNPs were dissolved in the prepared CNT suspension and ultrasonically oscillated for 12 h to obtain the CNTs/AgNPs solution. Finally, the CNTs/AgNPs solution was dropped onto the surfaces of SiO_2/Si substrate with spin coating, and the SERS substrates were placed in a nitrogen (N_2) atmosphere until the surfaces were evaporated to dryness. We roughly estimated that the actual weight percentage of AgNPs in the CNTs/AgNPs nanocomposite is about 43.2%.

2.2. SEM and TEM characterizations

The surface morphologies of the prepared samples were characterized by using a field emission scanning electron microscopy (FESEM, JEOL JSM-7800F). Low-magnification SEM characterization result of CNTs/AgNPs composite are shown in Fig. 2(a), and the enlarged SEM images are shown in Figs. 2(b)–2(d). It is observed that a large number of AgNPs were densely and uniformly deposited on the carbon nanotube films. In order to make a more intuitive comparison of the distribution of Ag nanoparticles, we calculated the particle sizes, numbers and other parameters of the three samples by Nano Measurement software, the corresponding results are shown in Figs. 2(e)–2(g).

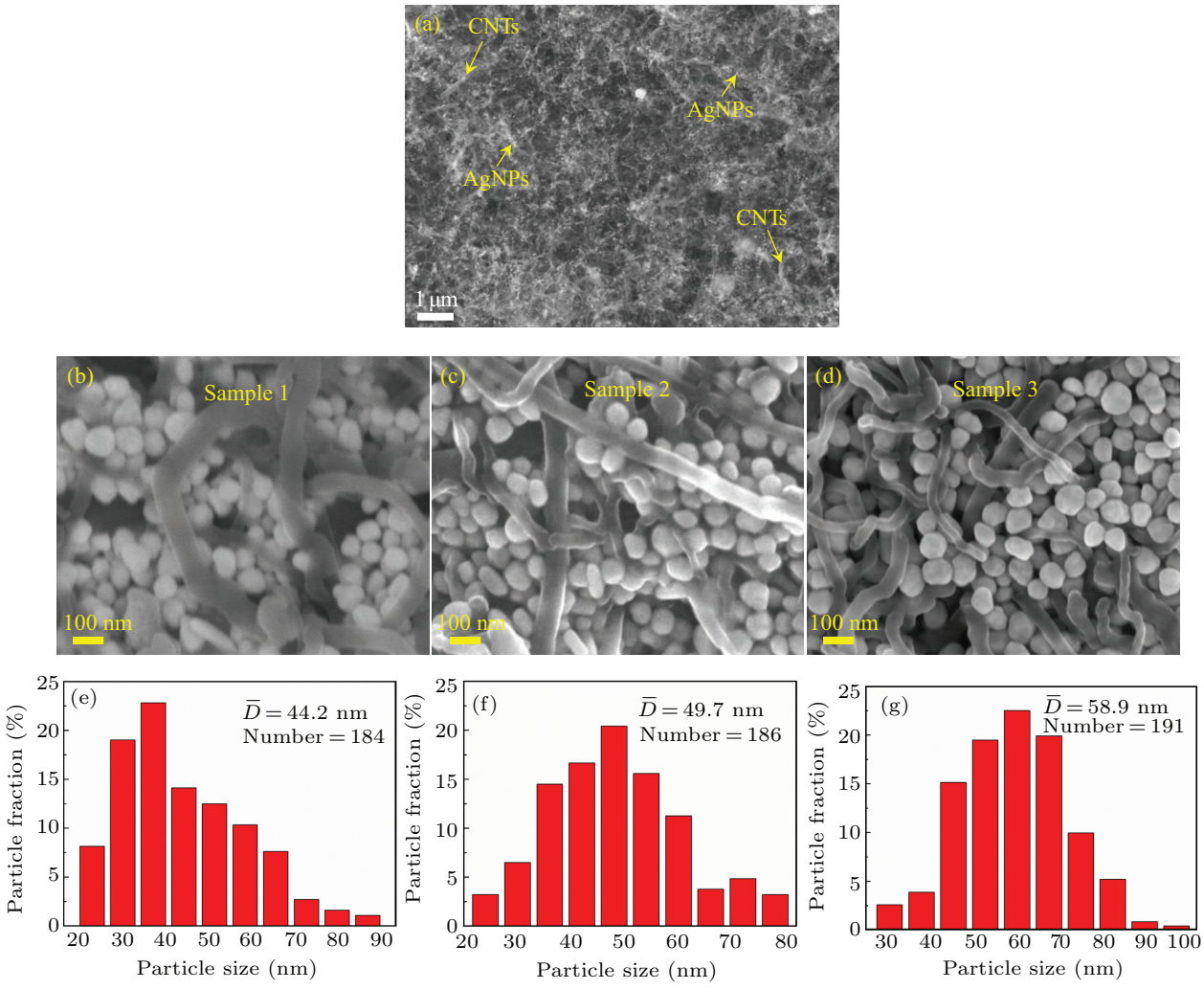


Fig. 2. (a) Low magnification SEM characterization result of CNTs/AgNPs composite; enlarged SEM image of (b) sample 1, (c) sample 2, and (d) sample 3. Corresponding size distribution of AgNPs in (e) sample 1, (f) sample 2, and (g) sample 3.

The statistical results show that (i) Ag nanoparticle size distribution ranges of sample 1 (25-mg sodium citrate), sample 2 (15-mg sodium citrate), and sample 3 (5-mg sodium citrate) are 20.5 nm–89.9 nm, 21.2 nm–80.1 nm, and 25.3 nm–101.6 nm, respectively, the average sizes of Ag nanoparticles are about 44.2, 49.7, and 58.9 nm, respectively. The size of AgNP increases with the amount of sodium citrate decreasing; (ii) in the area of 3 μm^2, the calculated numbers of AgNPs of the three samples are about 184, 186, and 191, respectively.

A low-magnification bright-field transmission electron microscopy (TEM) image of CNTs/AgNPs substrate is shown in Fig. 3(a), the CNTs are coated with Ag nanoparticles of diameter ranging from 20 nm to 80 nm, and most of the nanoparticles are spherical in shape. Figure 3(b) shows the high-resolution TEM (HRTEM) image of CNTs, the measured outer diameter of CNTs is 50.8 nm, the fringe lattice shown in the inset of Fig. 3(b) is about 0.34 nm, attributed to the (002) plane in CNT walls. Figure 3(c) shows the HRTEM image of Ag nanoparticles embedded on the CNTs, the measured fringe lattice of Ag nanoparticle shown in the inset of Fig. 3(c) is about 0.24 nm, which corresponds to the (111) crystal plane. Figure 3(d) shows a selected area electron diffraction (SAED) pattern of the hybrid, proving that the Ag nanoparticles are crystalline. Besides the innermost ring, which belongs to CNT, the other four bright rings are indexed, respectively, to cubic fcc (111), (200), (220), and (311) lattice plane of Ag metal from the inside to the outside.[35]

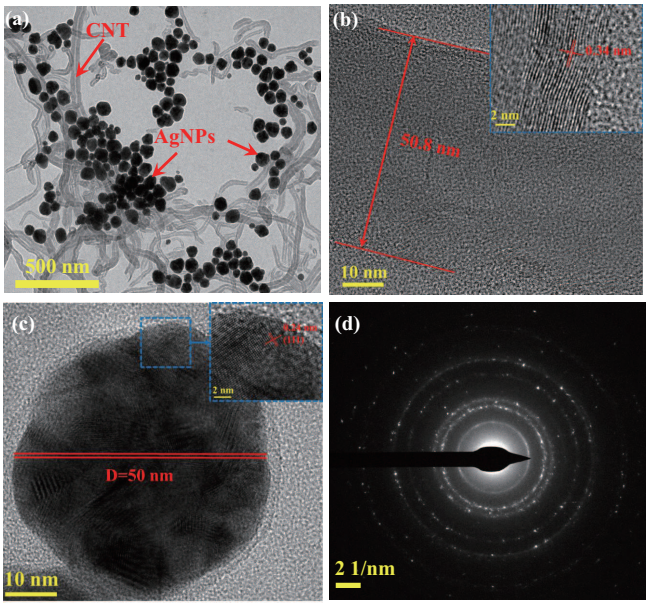


Fig. 3. TEM images of typical AgNPs decorated on the CNTs: (a) low-magnification TEM image of CNTs/AgNPs, HRTEM images of (b) CNTs and (c) AgNPs, (d) corresponding SAED of CNTs/AgNPs.

3. Experimental results and discussion

The absorption spectra of CNTs/AgNPs samples with different AgNPs sizes are examined over wavelengths ranging from 200 nm to 800 nm by using an ultraviolet-visible (UV-vis) spectrophotometer (Hitachi High-Tech U-3600). The Raman spectra are collected by using a laser confocal Raman spectrometer (Horiba Jobin Yvon LabRAM HR Evolution) with an incident wavelength of 532 nm, power of 50 mW and 10% filter, at room temperature. An integration time of 2 s is used in the measurements to reduce the heating effect induced by laser. The SERS measurements are carried out with R6G as probe molecules.

3.1. UV-vis absorption spectra of CNTs/AgNPs

The absorption properties of CNTs/AgNPs suspensions in water with AgNPs of different sizes are shown in Fig. 4. As indicated in Fig. 4, in the range of 200 nm–800 nm, there appear two different absorption characteristic peaks: one exists in a range between about 270 nm–275 nm, and the other is at about 419 nm. The former corresponds to the UV-vis absorption peak of carbon nanotubes, which is ascribed to the π–π^* electronic transition in C=C bonds of carbon nanotube structure,[36] the latter refers to the absorption characteristic peak of AgNPs, located at the LSPR wavelength of AgNPs. In addition, we also find that the absorptions of CNTs/AgNPs with different AgNP sizes are different, which is related to the concentrations of CNTs/ AgNPs sample. More importantly, with the increase of the Ag nanoparticle size, the characteristic peak of CNT has a red shift, which may result from the electronic interaction of molecular orbitals between carbon nanotubes and nanoparticles, constructing a new molecular orbit and reducing the band gap.[37]

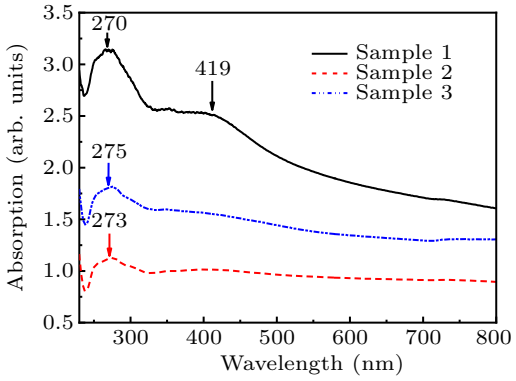


Fig. 4. UV-vis absorption spectra of CNTs/AgNPs samples with different AgNPs sizes.

3.2. Raman spectra of CNTs/AgNPs

The carbon nanotubes and the prepared CNTs/AgNPs samples are characterized by Raman spectroscopy. The experimental results and their Lorentz fitting results are shown in Fig. 5. The Raman spectrum of carbon nanotubes in the 1000 cm^{-1}–1800 cm^{-1} shift segment has two obvious characteristic peaks: D peak and G peak, located at 1338 cm^{-1} and 1575 cm^{-1}, respectively. The D peak is the breathing mode caused by vibration of the *k*-point phonons, which is a

reflection of defects and disorder of carbon nanotubes, and the G peak denotes the E_{2g} stretching vibration of carbon atoms, whose mode is a non-dispersive Raman mode.[38]

As the sizes of AgNPs increase, the Raman intensity of the D peak and G peak of CNTs/AgNPs increase. The enhancement of D peak is due to the doping effect and the surface roughness of Ag, while the enhancement of G peak is attributed to the electromagnetic enhancement of AgNPs and the coupling effect of AgNPs and CNTs. In order to further quantitatively analyze the Raman enhancement characteristics of the sample, the Raman frequency shift, intensity, and the values of full width at half maximum (FWHM) of the D peak and G peak of CNTs and CNTs/AgNPs samples are calculated. The results are summarized in Table 1, where I_D/I_G ratio is also presented. The intensity ratio I_D/I_G reflects the orderliness and integrity of the carbon nanotubes, and it is easily affected by chemical processes of CNTs and silver. The calculations of CNTs and the three CNTs/AgNPs samples of I_D/I_G are 0.61, 1.12, 1.14, 1.22, which indicate that as the size of AgNPs increases, the I_D/I_G ratio value increases, mainly because the deposition of AgNPs may affect the lattice vibration modes of CNTs.

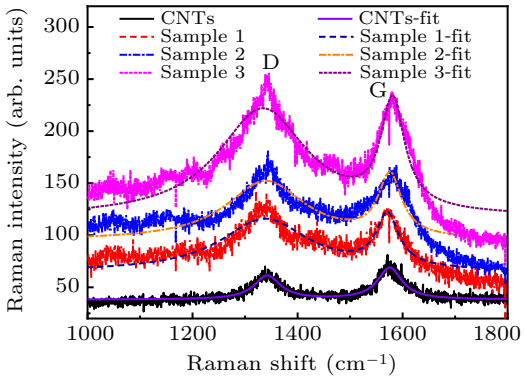


Fig. 5. Raman spectra of CNTs and three CNTs/AgNPs samples.

Table 1. Raman positions, intensities, FWHMs of CNTs, and three samples.

Samples	Position (cm^{-1})		Intensity (counts)		FWHM (cm^{-1})		I_D/I_G
	D	G	D	G	D	G	
CNTs	1338	1575	31.7	51.8	28	36	0.61
Sample 1	1340	1577	58.7	51.6	50	50	1.12
Sample 2	1343	1580	71.2	62.7	35	27	1.14
Sample 3	1346	1581	139.6	114.8	50	50	1.22

To evaluate the uniformity of the CNTs/AgNPs substrate (sample 3), we collect Raman spectra from randomly-selected region within an area of 10 μm×10 μm with a spacing of 1 μm on the CNTs/AgNPs substrate. In this experiment, the grating of the Raman spectrometer changes to 600 gr/mm, the integration time is set to be 1 s, keeping remaining test conditions the same as those in previous experiments (in general, the grating is set to be 1800 gr/mm). The Raman intensity mappings of G band and I_D/I_G are given in Fig. 6. The Raman intensities of G band are in a range of 250 counts–650 counts, and I_D/I_G values are in a range of 1.00–1.16, which indicates that our substrate is not sufficiently uniform. The reasons could be as follows. (i) The CNTs have poor dispersibility, and thus resulting in non-uniform dispersion of AgNPs deposited on the CNTs. (ii) The sizes of AgNPs deposited on the CNTs are not completely identical, and the nanogaps between two nanoparticles are not entirely equal either, thereby leading the hot spots to be distributed unevenly on the CNTs/AgNPs substrate. (iii) The roughness of CNTs surface is not uniform due to the deposition of AgNPs.

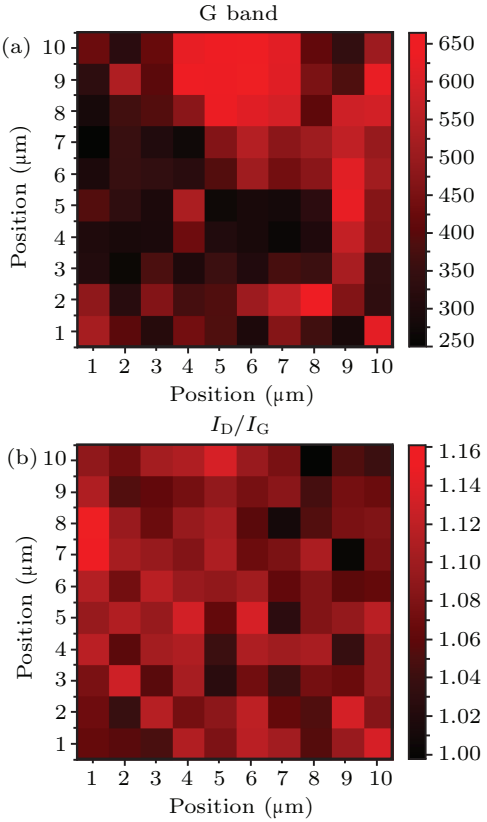


Fig. 6. Raman intensity mappings of (a) G band and (b) I_D/I_G.

3.3. SERS activity of CNTs/AgNPs

We compared Raman intensity of R6G at a concentration of 10^{-9} mol/L collected on pure CNTs, pure AgNPs, and CNTs/AgNPs as shown in Fig. 7. We can see that the Raman intensity collected on CNTs/AgNPs is larger than that collected on pure Ag nanoparticles. For Raman peak position at 1363 cm^{-1} and 1509 cm^{-1}, the Raman intensity collected on CNTs/AgNPs is about 4 fold higher than that collected on AgNPs substrate. The reasons could be as follows. (i) The enhancement induced by the coupling effect between CNTs and Ag nanoparticles is stronger than that between two silver nanoparticles, which results in greater Raman intensity. (ii) The total surface area of the carbon nanotubes is about 1.5 times larger than that of the planar area,[39] which indicates that the number of AgNPs adsorbed on CNTs is more than

that on the planar substrate, which can also enhance the Raman intensity.

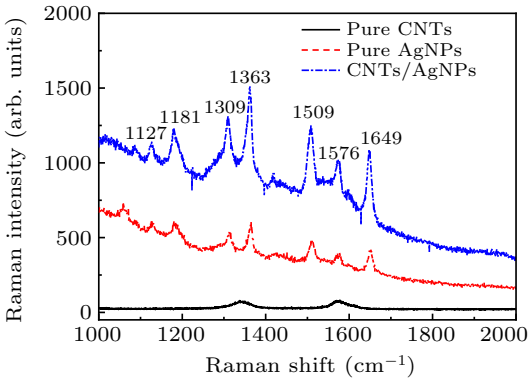


Fig. 7. Comparison among SERS spectra of 10^{-9} mol/L R6G on pure CNTs, pure AgNPs, and CNTs/AgNPs.

To estimate the SERS activity of the prepared CNTs/AgNPs substrate, Raman spectra of R6G molecules with a concentration of 10^{-10} mol/L on the CNTs/AgNPs nanostructures are measured, and the results are shown in Fig. 8. In the range of 1000 cm^{-1}–1800 cm^{-1}, most of R6G characteristic peaks can be obtained, but the Raman intensities of characteristic peaks are obviously different. At the Raman shifts of 1363 cm^{-1} and 1509 cm^{-1}, the Raman intensities increase more obviously. Meanwhile, within the experimental range, it can be found that the SERS signals of R6G increase orderly in the sequence of sample 1, sample 2, and sample 3, that is to say, the Raman intensities on CNTs/AgNPs substrates at different characteristic peaks for R6G increase gradually with AgNPs size increasing. For example, at $\sim$ 1363 cm^{-1} of R6G, the signals for sample 1, sample 2, and sample 3 are about 40, 160, and 370 counts, respectively. The intensity of sample 2 is thrice higher than that of sample 1, and the intensity of sample 3 is 8.25 times higher than that of sample 1 and 1.31 times higher than that of sample 2. The change of SERS intensity is attributed to the difference in size among Ag nanoparticles on the CNTs films obtained from different amounts of sodium citrate. In our experiments, the SERS intensity is dependent on the size of Ag nanoparticles, which can be controlled by varying the amount of sodium citrate.

The SERS enhancement factor (EF) is usually defined as $EF = (I_{\mathrm{SERS}}/I_{\mathrm{RS}})/(N_{\mathrm{SERS}}/N_{\mathrm{RS}})$.[40] In our experiments, the carbon nanotube films are not easily separated, meanwhile, the effective number of R6G molecules adsorbed on the CNTs/AgNPs substrate is difficult to accurately determine. Here, it is assumed that the R6G molecules are uniformly adsorbed on the surface of CNTs/AgNPs substrate. Therefore, the experimental enhancement factor can be calculated from the following formula: $EF = (I_{\mathrm{SERS}}/I_{\mathrm{RS}})/(C_{\mathrm{SERS}}/C_{\mathrm{RS}})$, where I_{SERS} and C_{SERS} are the Raman intensity and concentration for the SERS measurement (on CNTs/AgNPs substrate, 10^{-10} mol/L), respectively, I_{RS} and C_{RS} are the Raman intensity and concentration of corresponding peak for normal Raman measurement (on SiO_2/Si substrate, 10^{-2} mol/L), respectively.

The calculated EF values of CNTs/AgNPs samples are shown in Table 2. The EF values are different for different samples, even different for different Raman peaks of the same sample.

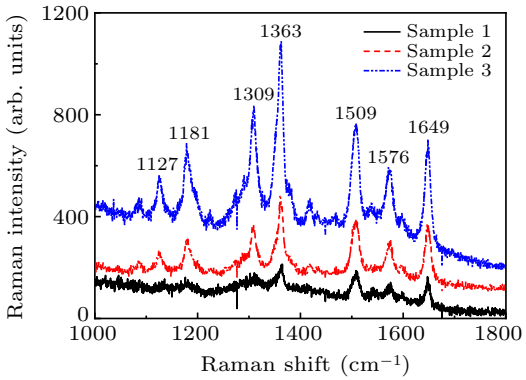


Fig. 8. SERS spectra of R6G at a concentration of 10^{-10} mol/L collected on CNTs/AgNPs.

Table 2. Calculation results of I_{RS}, I_{SERS}, and enhancement factor.

Peak position (cm^{-1})		1363	1509	1649
Sample 1	I_{RS} (arb. units)	233	92	196
	I_{SERS} (arb. units)	100	112	133
	EF	4.3×10^7	1.2×10^8	6.8×10^7
Sample 2	I_{SERS} (arb. units)	283	252	270
	EF	1.2×10^8	2.7×10^8	1.4×10^8
Sample 3	I_{SERS} (arb. units)	697	412	437
	EF	3.0×10^8	4.5×10^8	2.2×10^8

4. FDTD simulation analysis

4.1. Extinction, scattering and absorption of AgNPs with different particle sizes

The finite difference time domain (FDTD) approach is one of the widely used numerical simulation methods in electromagnetics and micro/nano optics since it was proposed by Yee in 1966.[41] The FDTD method involves the discretization of Maxwell's equations in time and space domain, and uses the precision of the finite difference to achieve an accurate solution of the electromagnetic field. This method can be conveniently used to simulate various kinds of scattering, diffractions and radiation propagations by adjusting the number, size and material properties of the Yee cell.[42]

In this work, we studied the scattering and absorption properties of Ag nanoparticles with different nanoparticle sizes by the FDTD method using the Mie theory. The surrounding medium was set to be 1.0 ($n_{\mathrm{medium}} = 1.0$), and the diameter range of AgNPs was set to be 20 nm–80 nm. The relationship between the calculated scattering and absorption cross sections and wavelengths are shown in Figs. 9(b) and

9(c), the extinction cross section is given by $\sigma_{ext} = \sigma_{sca} + \sigma_{abs}$ as shown in Fig. 9(a). We can clearly find that the positions of the maximum extinction, scattering and absorption peaks are red-shifted as the AgNPs size increases, as well as the surface plasmon resonance (SPR) wavelengths. Larger silver nanospheres have larger scattering cross-section, and shows much broader plasmon bandwidth, which can be explained in theory.[43,44] The larger the particles become, the more important the higher order oscillation modes are because the light can no longer polarize the nanoparticles homogeneously.[45] As a consequence, retardation effects of the electromagnetic field across the particle can cause the surface plasmon resonances to shift. These higher order modes peak at lower energy, and therefore, the plasmon band red-shifts with particle size increasing. The relationship between the AgNPs size and SPR wavelength is shown in Fig. 9(d), and different sizes of AgNPs (20 nm–80 nm) correspond to different SPR wavelengths (360 nm–385 nm). The sphere diameter has fundamental linear relation with the SPR wavelength of AgNPs, the obtained formula is $\lambda_{SPR} = 0.1456 \times D_{Ag} + 350$, and the correlation coefficient $R^2 = 0.96445$.

According to the above simulation results, the LSPR wavelengths of AgNPs are 360 nm–385 nm. Theoretically, the closer to the peak of LSPR the excitation wavelength, the better the SERS activity is, but the LSPR wavelength is where the absorption peak of far field is located, which reflects the average information of Ag nanoparticles in the spot. The electromagnetic field is a near-field distribution that reflects the coupling information of the metal nanoparticles. In our previous simulation results, the 532-nm excitation source obtained the highest electromagnetic field strength. Therefore, in the latter simulation, the excitation wavelength is selected to be 532 nm.

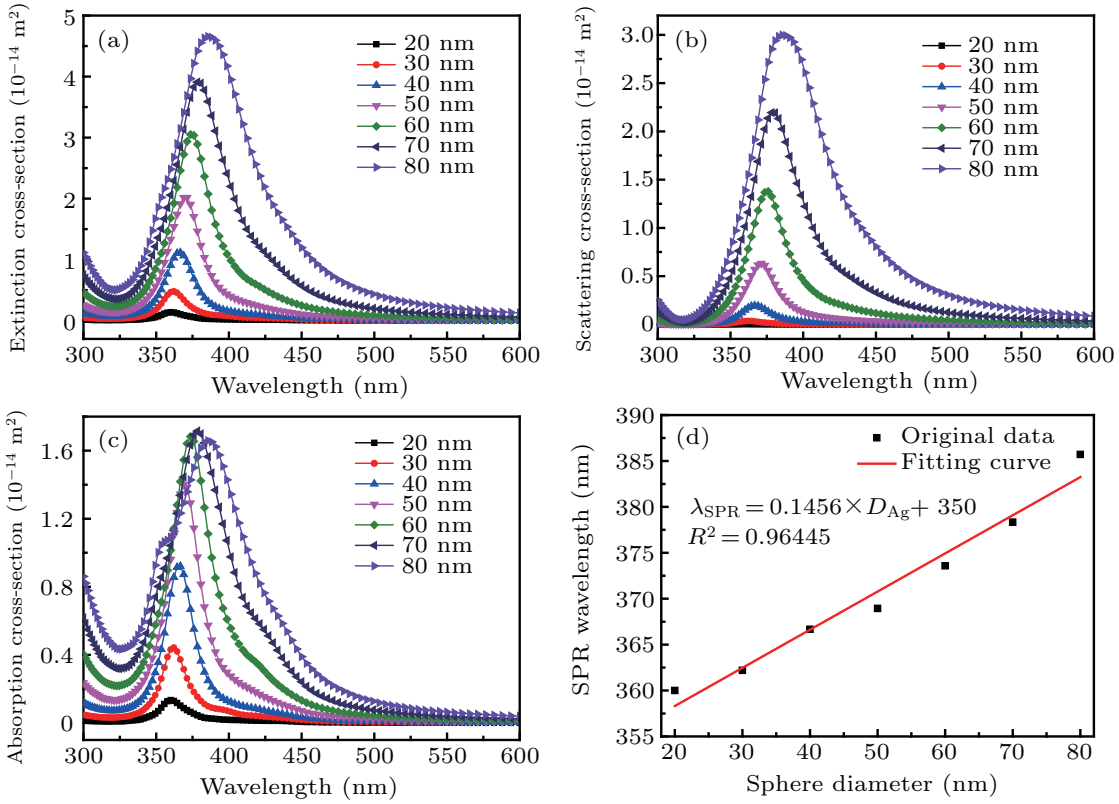


Fig. 9. (a) Extinction, (b) scattering, and (c) absorption cross sections of AgNPs with difference sizes ($n_{medium} = 1.0$); (d) Relationship between AgNPs size and SPR wavelength.

4.2. Simulation analysis of CNTs/AgNPs

In addition, we numerically analyzed the influences of AgNPs sizes on the electric field enhancement and distribution of CNTs/AgNPs composites by the FDTD method. We simulated a system formed by a nanotube with 20-nm inner diameter and 50-nm outer diameter, with the nanotube separated by 0.5 nm from two Ag nanospheres with different sizes (both on a 300-nm SiO_2 film). According to the previous experimental results, the diameter of AgNPs was set to be 44, 50, and 59 nm, separately, and the nanogap between adjacent nanoparticles was set to be 2 nm. In the simulation, we chose multi-walled metallic CNTs, whose respective dielectric permittivity and refractive index functions are cited from Ref. [46] as plotted in Fig. 10. The simulations were carried out in air circumstance ($n_{medium} = 1.0$), and the incident light was set to be 532 nm in wavelength and propagates in the z-backward mode, *i.e.*, the incident light is x-polarized and travels along the z direction, and the incident field intensity is $E_0 = 1$ V/m.

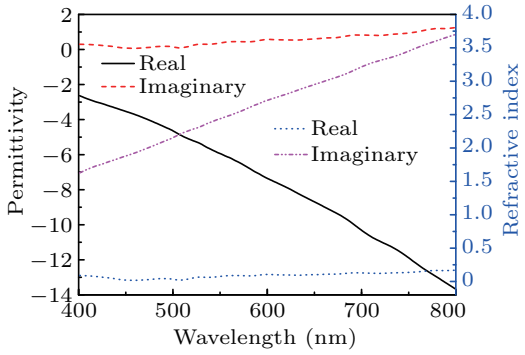


Fig. 10. Corresponding dielectric permittivity and refractive index functions of metallic CNTs.

4.2.1. Simulation in air circumstance

The electric field distributions of CNTs/AgNPs with different AgNPs sizes are shown in Figs. 11(b)–11(d). We can see in Fig. 11(d) that there are two kinds of hot spots, which are shown with red arrows; one exists between CNTs and AgNPs, the corresponding intensity curves along the x direction are shown in Fig. 11(e), the maximum electric field intensities of the three samples are about 84.90 V/m, 93.12 V/m, and 105.11 V/m, respectively; and the other exists near the AgNPs on CNTs surface, whose corresponding intensity curves along the x direction are shown in Fig. 11(f), from which we can see that the maximum electric field intensities are about 44.68 V/m, 62.75 V/m, and 86.35 V/m, respectively. Comparing Fig. 11(e) with Fig. 11(f) we can find that the electric field intensity in Fig. 11(e) is stronger than in Fig. 11(f). The maximum electric field intensities $E_{\max}$ of the coupling effect between two AgNPs increase in the following order: D_{Ag} (44 nm) < D_{Ag} (50 nm) < D_{Ag} (59 nm), which indicates that as the AgNPs size increases, the maximum electric field intensity increases, resulting in greater enhancement effect.

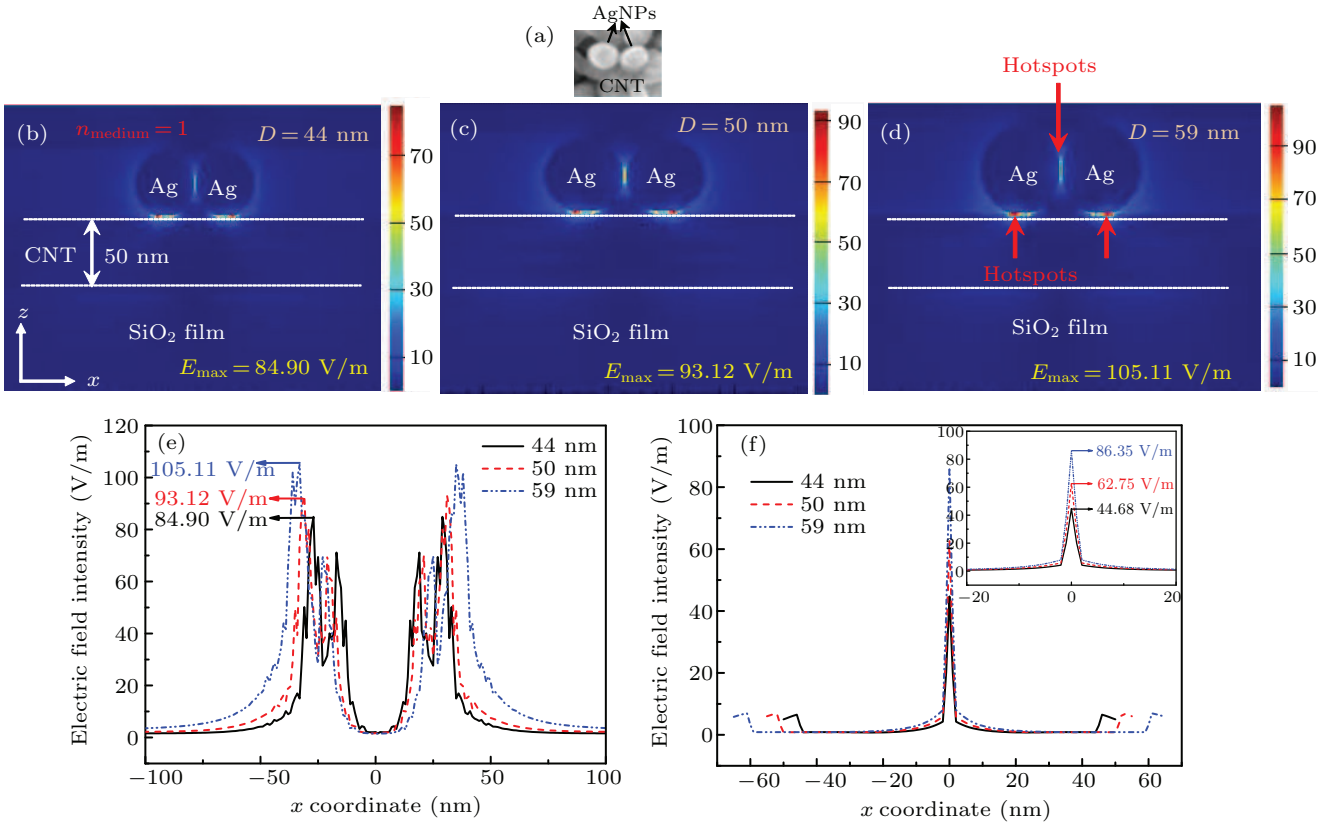


Fig. 11. (a) SEM image of CNTs/AgNPs on SiO_2/Si. SEM image of electric field distributions of CNTs/AgNPs samples, AgNPs diameter of (b) 44 nm, (c) 50 nm, and (d) 59 nm. (e) Intensities of hot spots between CNTs and AgNPs along x direction, (f) intensity between two AgNPs along x direction. The simulation of the surrounding medium is $n_{\mathrm{medium}} = 1.0$.

We calculated and found the total $E_{\max}$ values of sample 2 and sample 3 are increased by 9.68% and 23.8% compared with that of sample 1. According to the mechanism of electromagnetic enhancement, the electromagnetic enhancement factor can be obtained from[47]

$$EF_{\mathrm{EM}} = \frac{|E_{\mathrm{out}}|^2 |E'_{\mathrm{out}}|^2}{|E_0|^4},$$

where E_0 is the incident electric field intensity, $E_0 = 1$ V/m, and E_{out} is the electric field intensity of the position of hot spots caused by the incident light, E'_{out} refers to the field evaluated at the scattering frequency. The local electric field intensity of SERS ($|E_{\mathrm{out}}|^2 \times |E'_{\mathrm{out}}|^2$) is approximately equal to the surface localized electric field intensity of nanoparticles ($|E_{\mathrm{out}}|^4$). Therefore, the above formula can be changed into $EF_{\mathrm{EM}} = \frac{|E_{\mathrm{out}}|^4}{|E_0|^4}$. For $D_{\mathrm{Ag}} = 44$ nm, we have $EF_{\mathrm{EM}} = 84.90^4 \approx 5.2 \times 10^7$, for $D_{\mathrm{Ag}} = 50$ nm, and $EF_{\mathrm{EM}} = 93.12^4 \approx 7.5 \times 10^7$, and for $D_{\mathrm{Ag}} = 59$ nm, $EF_{\mathrm{EM}} = 105.11^4 \approx 1.2 \times 10^8$. From the calculated results of EF_{EM}, we found that the EF_{EM} values of

sample 2 and sample 3 are increased by 32.7% and 130% compared with that of sample 1, that the $EF_{\rm EM}$ value of sample 3 is increased by 60% compared with that of sample 2. The simulation results show that the tendency is consistent with the experimental result.

4.2.2. Simulation in real R6G solution

In our Raman test, 10^{-10} mol/L aqueous solution of R6G was chosen as the probe molecules. In order to make the parameters set in the simulation consistent with the experimental parameters, we used Abbe refractometer to measure the refractive index of water and different concentrations of R6G (10^{-6} mol/L$\sim 10^{-12}$ mol/L), and obtained the refractive index of water was 1.3320, and the refractive index of R6G was in the range of 1.3342$\sim$1.3348. Therefore, in our simulation analysis, the refractive index of surrounding medium was approximately set to be water's refractive index, $n_{\rm medium} = 1.33$. The simulation model, parameters and conditions are not charged. Simulated results are shown in Fig. 12. We also can see that there are two kinds of hot spots, one existing between CNTs and AgNPs and the other existing between the adjacent AgNPs on CNTs surface, but the latter is stronger than the former, which is contrary to the previous results of $n_{\rm medium} = 1.0$. In addition, the maximum electric field intensities of the three samples (sample 1, $D_{\rm Ag} = 44$ nm, shown in Fig. 12(a); sample 2, $D_{\rm Ag} = 50$ nm, shown in Fig. 12(b); sample 3, $D_{\rm Ag} = 59$ nm, shown in Fig. 12(c)) are 185.99 V/m, 209.72 V/m, and 216.40 V/m, respectively. Compared with the previous results of $n_{\rm medium} = 1.0$, there is an increase of 119%, 125%, and 106%, respectively. The main reason could be: as the surrounding refractive index increases, the scattering cross section and intensity increase, resulting in an increase in the field enhancement. According to the $EF_{\rm EM}$calculation formula, the corresponding $EF_{\rm EM}$ values of the three samples are about $EF_{\rm EM} = 185.99^4 \approx 1.2 \times 10^9$, $EF_{\rm EM} = 209.72^4 \approx 1.9 \times 10^9$, $EF_{\rm EM} = 216.40^4 \approx 2.2 \times 10^9$, respectively. From the calculated results of $EF_{\rm EM}$, we found that the $EF_{\rm EM}$ values of sample 2 and sample 3 were increased by 58.3% and 83.3% compared with the sample of 1, sample 3 was increased by 15.8% compared with the sample of 2. The simulation shows that the trend is consistent with the experimental.

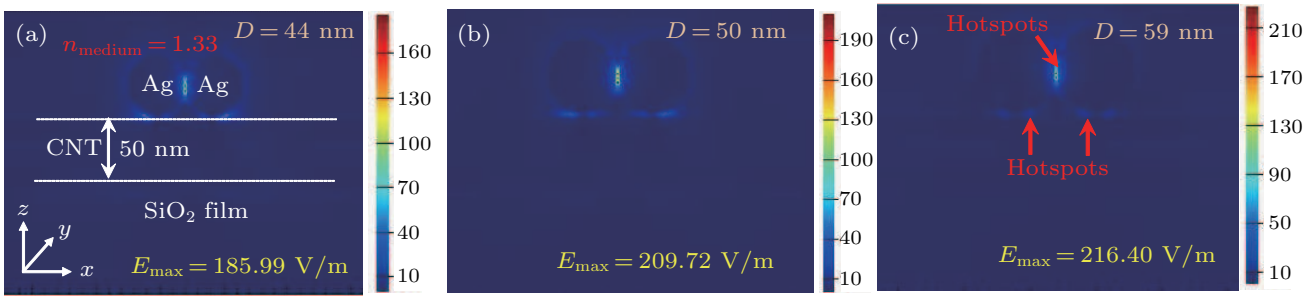


Fig. 12. Electric field distribution of AgNPs with diameter of (a) 40 nm, (b) 50 nm, and (c) 60 nm. In simulation $n_{\rm medium} = 1.33$.

In order to compare the simulation results with experimental results, the simulation $EF_{\rm EM}$ values and experimental EF values of the three CNTs/AgNPs samples are obtained as shown in Table 3. We can find that: i) $n_{\rm medium} = 1.33$, the simulation results are larger than the experimental ones, which could be due to the fact that the nanogap between two AgNPs in simulation is smaller than the experimental one. In addition, in the simulations and experiments, the surrounding medium environment of CNTs/AgNPs is not exactly consistent; ii) more importantly, the EF values of simulation and experimental EF values both increase with the size of AgNPs rising, and the relationship between them is basically linear.

Table 3. Comparison between experimental results and simulation results of three CNTs/AgNPs samples.

Samples	Experiment results (maximum)	Simulation results ($n_{\rm medium} = 1.0$)	Simulaiton results ($n_{\rm medium} = 1.33$)
Sample 1	1.2×10^8	5.2×10^7	1.2×10^9
Sample 2	2.7×10^8	7.5×10^7	1.9×10^9
Sample 3	4.5×10^8	1.2×10^8	2.2×10^9

5. Conclusions

In this work, we prepared Ag nanoparticles modified carbon nanotube composite structures with different sizes by simple and low-cost chemical reduction and self-assembling methods, and analyzed the Raman characteristics and SERS activities of CNTs/AgNPs samples with different sizes of Ag nanoparticles. In addition, we simulated the electric field distributions of CNTs/AgNPs samples by the FDTD method, and obtained two kinds of hot spots which contribute to the $EF_{\rm EM}$ by about 2.2×10^9, close to the experimental value of 4.5×10^8. Future work will focus on preparing the AgNPs with range sizes (by controlling the amount of sodium citrate and silver nitrate), and also on increasing the uniformity of AgNPs coated on the CNTs.

Acknowledgements

We would like to thank Mr. Xiangnan Gong from Analytical and Testing Center of Chongqing University for the help with Raman spectrometer.

Project supported by the National Natural Science Foundation of China (Grant No. 61875024), the Natural Science Foundation of Chongqing, China (Grant Nos. cstc2019jcyj-msxmX0639 and cstc2020jcyj-msxm0605), and the Scientific and Technology Research Program of Chongqing Municipal Education Commission, China (Grant Nos. KJQN202000648 and KJQN201900602).

References

[1] Raman C V and Krishnan K S 1928 *Nature* **121** 501
[2] Fleischmann M, Hendra P J and McQuillan A J 1974 *Chem. Phys. Lett.* **26** 163
[3] Park H J, Hwang K O and Kim E S 2002 *J. Microbiol. Biotechnol.* **12** 706
[4] Chen Y and Liu L 2014 *Plasmonics in Biology and Medicine XI* **895702** 8957
[5] He L L, Kim J N and Li H 2008 *J. Agric. Food Chem.* **56** 9843
[6] Liu B, Zhou P, Liu X M, Sun X, Li H and Lin M S 2013 *Food Bioprocess Tech.* **6** 710
[7] Chen L M and Liu Y N 2011 *ACS Appl. Mater. Interfaces* **3** 3091
[8] Bartlett P and Mahajan S 2012 *Advances in Electrochemical Science and Engineering: Bioelectrochemistry* **13**
[9] Schlücker S 2014 *Angew. Chem. Int. Ed.* **53** 4756
[10] Kneipp J, Kneipp H and Kneipp K 2008 *Chem. Soc. Rev.* **37** 1052
[11] Kneipp K, Wana Y and Kneipp H 1997 *Phys. Rev. Lett.* **78** 1667
[12] Campion A and Kambhampati P 1998 *Chem. Soc. Rev.* **27** 241
[13] Moskovits M 2005 *J. Raman Spectrosc.* **36** 485
[14] Tame M S, McEnery K R, Ozdemir S K, Lee J, Maier S A and Kim M S 2013 *Nat. Phys.* **9** 329
[15] Lin K, Yi J, Hu S, Liu B, Liu J, Wang X and Ren B 2016 *J. Phys. Chem. C* **120** 20806
[16] Benz F, Chikkaraddy R, Salmon A, Ohadi H, Nijs B, Mertens J, Carnegie C, Bowman W R and Baumberg J J 2016 *J. Phys. Chem. Lett.* **7** 2264
[17] Cassar R N, Graham D, Larmour I, Wark A W and Faulds K 2014 *Vib. Spectrosc.* **71** 41
[18] Lin W H, Cao E, Zhang L Q, Xu X F, Song Y Z, Liang W J and Sun M T 2018 *Nanoscale* **10** 5482
[19] Wang J G, Cao E, Lin W and Sun M T 2020 *Appl. Spectrosc. Rev.* **55** 558
[20] Cao Y, Cheng Y Q and Sun M T 2021 *Appl. Spectrosc. Rev.* **1**
[21] Gong T C, Zhu Y, Zhang J, Ren W J, Quan J M and Wang N 2015 *Carbon* **87** 385
[22] Ding G, Xie S, Liu Y, Wang L and Xu F G 2015 *Appl. Surf. Sci.* **345** 310
[23] Hsu K C and Chen D H 2015 *ACS Appl. Mater. Inter.* **7** 27571
[24] Zhang J, Zhang X L, Ding Y M and Zhu Y 2016 *Appl. Opt.* **55** 9105
[25] Zhai Y, Yang H, Zhang S N, Li J H, Shi K X and Jin F J 2021 *J. Mater. Chem. C.* **9** 6823
[26] Guo T J, Ding F S, Li D L, Zhang W, Cao L R and Liu Z M 2019 *Appl. Sci.* **9** 398
[27] Sun N, Wang Z K, Jiang M and Zhang J 2021 *Opt. Mater. Expr.* **11** 1321
[28] Singh D K, Iyer P K and Giri P K 2012 *Carbon* **50** 4495
[29] Bondarev I V and Gulyuk A V 2015 *Superlattice Microst.* **87** 103
[30] Zhang J, Zhang X L, Chen S M, Gong T C and Zhu Y 2016 *Carbon* **100** 395
[31] Liu C D, Wang L, Guo Y, Gao X, Xu Y Y, Wei Q, Man B Y and Yang C 2019 *Appl. Surf. Sci.* **487** 1077
[32] Xu Y R, Zhao X G, Jiang J and Zhang X 2019 *Nanoscale* **11** 7572
[33] Wei H N, Peng Z S, Yang C, Tian Y, Sun L F, Wang G T and Liu M 2021 *Nanomaterials* **11**
[34] Lee P C and Meisel D 1982 *J. Phys. Chem.* **86** 3391
[35] Cui S M, Pu H H, Lu G.H, Wen Z H, Mattson E C C and Chen W J H 2012 *ACS Appl. Mater. Inter.* **4** 4898
[36] Rance G A, Dan H M, Nicholas R J and Khlobystov A N 2010 *Chem. Phys. Lett.* **19** 493
[37] Mohammed M K A, Ahmed D S and Mohammad M R 2019 *Mater. Res. Express* **6** 055404
[38] Kudin K N, Ozbas B, Schniepp H C, Prud-Homme R K, Aksay I A and Car R 2008 *Nano Lett.* **8** 36
[39] Zhang J, Fan T, Zhang X L, Lai C H and Zhu Y 2014 *Appl. Opt.* **53** 1159
[40] Le Ru E C, Blackie E, Meyer M and Etchegoin P G 2007 *J. Phys. Chem. C* **111** 13794
[41] Yee K S 1966 *IEEE Trans. Antennas Propag.* **14** 302
[42] Oubre C and Nordlander P 2005 *J. Phys. Chem. B* **109** 10042
[43] Bohren F C and Huffman D R 1983 Wiley
[44] Pinchuk A, Hilger A, Plessen G V and Kreibig U 2004 *Nanotechnology* **15** 1890
[45] Sujit K G and Tarasankar P 2007 *Chem. Rev.* **107** 4797
[46] Cui X, Dong L, Zhang W, Wu W, Tang Y and Erni D 2010 *Appl. Phys. B.* **101** 601
[47] Zhao Y, Chen G, Du Y, Xu J, Wu S, Qu Y and Zhu Y 2014 *Nanoscale* **6** 13754